Industrial Chemistry & Materials

ROYAL SOCIETY OF CHEMISTRY

PAPER

View Article Online
View Journal

Cite this: DOI: 10.1039/d5im00019j

Effect of adsorbent loading on NaNiRu-DFMs' CO_2 capture and methanation: finding optimal Na-loading using Bayesian optimisation guided experiments†

Soudabeh Bahrami Gharamaleki,[a] Sergio Carrasco Ruiz,[b] Tomas Ramirez Reina,[b] Michael Short [a] and Melis S. Duyar *[a]

Received 30th January 2025,
Accepted 22nd April 2025

DOI: 10.1039/d5im00019j

rsc.li/icm

Designing dual function materials (DFMs) entails an optimisation of CO_2 adsorption and catalytic conversion activity, often requiring a large number of experimental parametric studies screening various types and loadings of adsorbent and catalyst components. In this study, we used a Gaussian process model optimised with Bayesian optimisation (BO) to find the DFM composition leading to the highest methanation activity. We focused on optimising Na (adsorbent) loading in a DFM where Na loading was varied from 2.5–15% by weight. The results from the experimental tests indicated that the sample with the highest Na-loading (15 wt%) possessed the highest CO_2 desorption during CO_2-TPD, however, it was not the best DFM, as it did not show the highest methane production. By testing Bayesian optimisation recommended experiments we identified 7.9 wt% Na as the optimal Na loading, which showed the highest methane production for a cycle (398.6 μmol g_{DFM}^{-1}) at 400 °C. This forms a case study for how BO can help accelerate materials discovery for DFMs.

Keywords: DFM; ICCC; Methanation; Gaussian process; Bayesian optimisation.

1 Introduction

Integrated CO_2 capture and conversion (ICCC) with the aid of dual function materials (DFMs) is gathering momentum as a potential solution to dealing with the rising amount of CO_2 in the atmosphere.[1–3]

ICCU using DFMs presents a promising approach for simultaneously mitigating carbon emissions and producing value-added chemicals or fuels.[4–7] This approach offers a cost-effective alternative to conventional, sequential processes. By utilising DFMs that combine CO_2 adsorption and catalytic functionalities, ICCU decreases energy consumption and capital investment while enhancing process efficiency.[8–10] Moreover, the tunability of DFMs allows for optimisation toward specific CO_2-derived products, such as methane, syngas, or methanol, through tailored adsorbent-catalyst compositions and operating conditions. This approach not only contributes to the circular carbon economy but also reduces the energetic and economic burdens associated with CO_2 capture and separate conversion stages, making it a viable strategy for industrial-scale carbon valorisation.[11,12]

DFMs have demonstrated remarkable capability of capturing CO_2 and converting it to methane.[13–15] However, there is still a need to improve the capture capacity of the DFMs using alkali/alkaline earth material as adsorbents.[16,17] Hence designing DFMs with high adsorption and conversion rates is of vital importance. Researchers have investigated various designs by alternating the adsorbents or catalytic materials in DFMs' structure sorbent.[18–26] The literature studied the Ru-based DFMs in various realistic conditions in CO_2 capture and methanation. Jeong-Potter *et al.*, reported that increasing the Ru loading from 0.1 to 1% can increase the methane production for Ru10Na/Al while the adsorption feed gas contains 400 ppm of CO_2, 21% O_2, and N_2 as balance.[17] They showed that the sample with 1Ru10Na/Al has stable methanation behaviour under realistic conditions (0.027 g g_{sample}^{-1}). Zheng *et al.* evaluated the effect of the various parameters (temperature, time of stream (TOS), feed flow rates) on the performance of 5Ru10Ca/Al DFMs with the feed gas containing: 7.5% CO_2, 15% steam, 4.5% O_2 and N_2 as balance.[27] They reported that the samples were producing methane under all the tested conditions. Lin *et al.*,

[a] *School of Chemistry and Chemical Engineering, University of Surrey, Guildford, UK. E-mail: m.duyar@surrey.ac.uk*
[b] *Inorganic Chemistry Department and Materials Sciences Institute, University of Seville, Seville, Spain*

† Electronic supplementary information (ESI) available: Dynamic H_2-TPSR and activity plots, GP and BO results. See DOI: https://doi.org/10.1039/d5im00019j

demonstrated that a monolith containing 0.25Ru6.1Na/Al is resistant under realistic conditions in CO_2 capture and methanation processes.[28] It showed a slight decrease in its performance after being aged for 250 hours (TOS) under various conditions using 400 ppm CO_2 per air. The produced methane was 400 μmol $g_{washcoat}^{-1}$. Our earlier study on 5Ru10Ca/Al also states that the sample was stable (300 μmol g^{-1}) after 20 CO_2 capture and methanation cycles using 8% CO_2, 21% H_2O, and balance air.[29] All of these studies showed the robustness of Ru-based in DFMs in the presence of realistic conditions and that could be associated with the fact that ruthenium can rapidly and reversibly transform between Ru and RuOx and oxidising (adsorption) and reducing (hydrogenation) environments. Sodium-based DFMs attract more attention when designing DFMs for methanation because of their satisfactory reversible adsorption/desorption capability at intermediate temperatures.[30,31] They also evaluate different loadings of effective materials on the performance of the DFM in the CO_2 capture and conversion process; however, to date, no computationally guided optimisation methodologies have been utilised in the context of DFMs' design.

DFM design commonly employs an experimental "screening" approach where the loading of components is systematically varied. Tsiotsias *et al.* studied varying the loading of Ru as the catalytic material in CO_2 capture and methanation with *X*RuNaAl (*X* = 0.25, 0.5, 1, 2, and 4 wt%). They reported that increased Ru loading promotes the production of CH_4 at lower temperatures. The highest CH_4 production capacity was reported as 0.97 mmol g^{-1} for 4RuNaAl DFM in the H_2-TPSR test.[32] In another study, Tsiotsias *et al.* investigated *X*Ru20NiNa/Al (*X* = 0, 0.1, 0.2, 0.5, and 1 wt%), and determined the sample with 0.2Ru20NiNa/Al showed the highest methane production at 300 °C with more than 500 μmol g_{DFM}^{-1} over 30 minutes of hydrogenation.[33] Vandelois also investigated the effect of Ru loading on *X*RuNa (1, 2, 4, and 5 wt%) DFMs' CO_2 capture and methanation performance. The study indicated that the higher the Ru loading the better the DFMs' performance in CH_4 production.[34] However, it is apparent that continuously increasing the Ru loading will not result in increasingly better performance due to the need to balance the number of sites with the efficiency with which Ru atoms participate in the reaction; in other words, there must be an optimal loading which was not screened in this study. This highlights the need for careful design of experiments to find optimised compositions of DFMs, which is an area where computational techniques can greatly speed up material discovery. In another study, Tsiotsias *et al.* investigated the influence of the weight ratio between the catalytic material and adsorbent in a series of monometallic and bimetallic DFMs for methanation: Ru–10Ni/Pr–CeO_2, Na_2O/Al_2O_3, and 10Ni/Pr–CeO_2, Na_2O/Al_2O_3 DFMs, in CO_2 adsorption and conversion to methane. They reported that the sample with 1:3 catalyst-to-adsorbent ratio in bimetallic DFM was the sample with the highest methane yield. The cumulative CH_4 yield was 0.45 (mmol g^{-1}) in 30 minutes.[35]

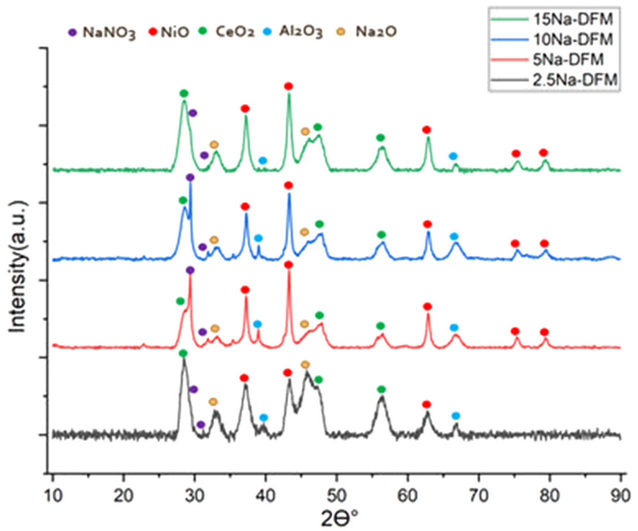

Fig. 1 XRD graphs of 15Ni1Ru*X*Na-DFMs (*X* = 2.5–15%).

In our early investigations into methanation DFMs we systematically screened the influence of varying adsorbent loadings (MgO, K_2CO_3, and Na_2CO_3) in DFMs where Ru was the methanation catalyst.[36] Adsorbent loadings were increased from 5% to 20% by weight to examine their effect on CO_2 capture capacity and the reversibility of the process. The results indicated that the DFM containing 20 wt% K_2CO_3 achieved the highest CO_2 capture capacity, while the DFM with 10 wt% Na_2CO_3 exhibited superior reversibility (leading to higher conversion of captured CO_2). Bermejo-López *et al.* evaluated varying the loading of the adsorbent material for Ru–*X*CaO/Al_2O_3 and Ru–*X*Na_2CO_3/Al_2O_3 (*X* = 5, 10, and 15 wt%) DFMs. They reported that the CO_2 capture and conversion performance of the DFMs improved by increasing

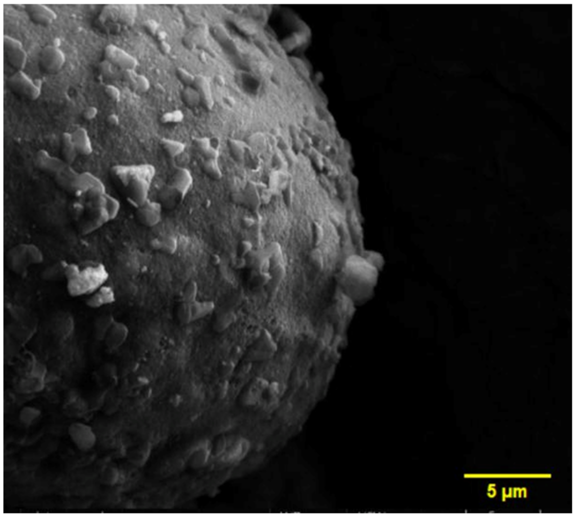

Fig. 2 SEM image of 15Ni1Ru, 15Na-DFM.

the adsorbent materials' loading and the highest methane production (414 μmol g^{-1}) was achieved by $Ru15CaO/Al_2O_3$ at 400 °C. The study also stated that higher Ru dispersion and lower carbonate stability in $Ru10Na_2CO_3/Al_2O_3$ enhances methane production at lower temperatures (383 μmol g^{-1} at 310 °C).[30] These findings highlight the significance of adsorbent composition and loading in optimising DFMs for effective CO_2 capture and utilisation, but it is not possible to

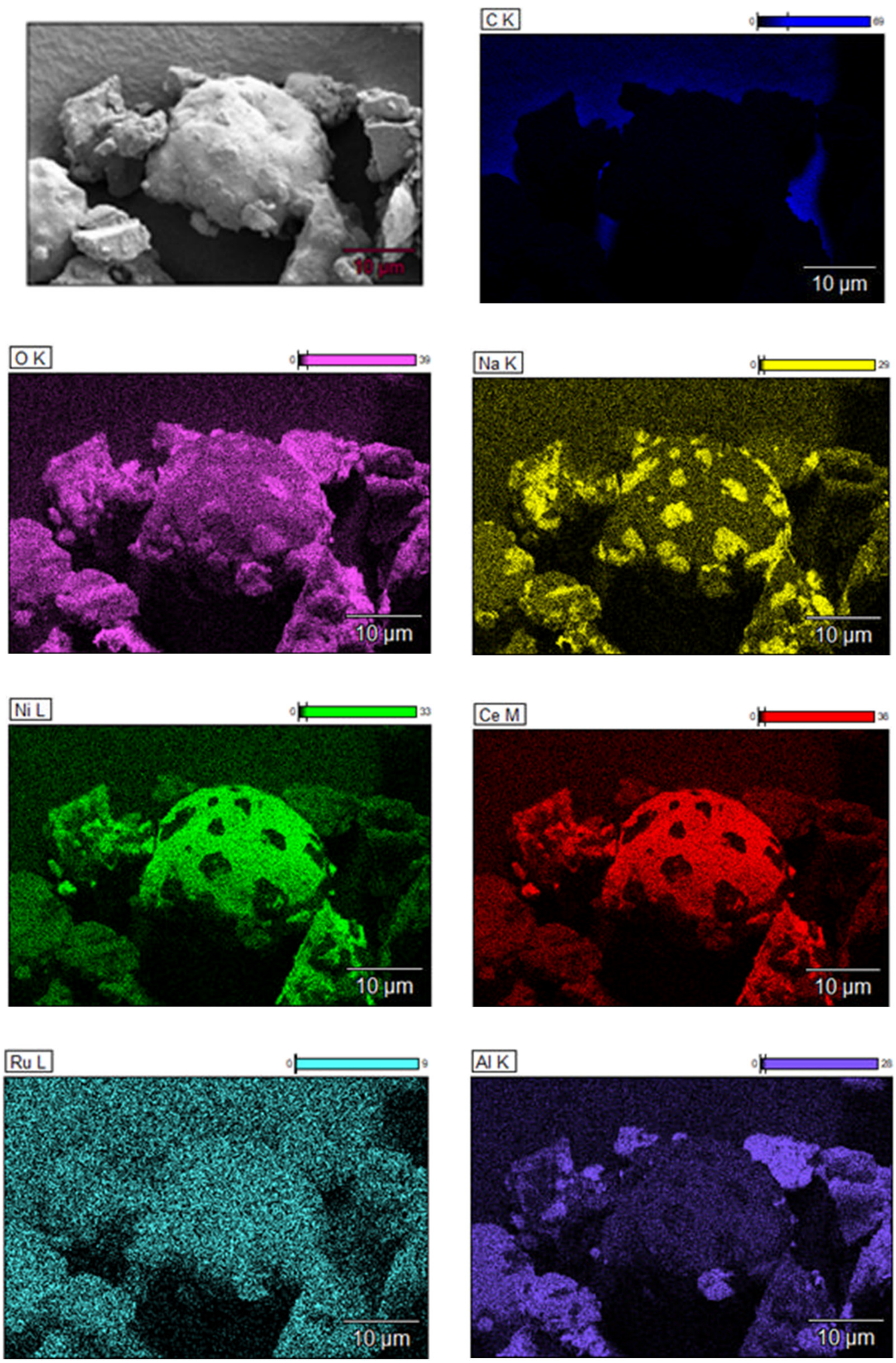

Fig. 3 EDS mapping of 15Ni1Ru, 15Na-DFM.

know from these where the true optimum sorbent composition is. The situation becomes even more complex if we wish to optimise the full dual function material (adsorbent, catalyst, support, and possibly promoters), and hence a computational optimisation approach to guide experimental efforts can greatly simplify the process of DFM design.

Bayesian optimisation (BO) is a data-driven technique that excels in modelling complex systems and optimising experimental processes with minimal resource expenditure. By building a surrogate model from experimental data with the aid of the Gaussian process (GP), Bayesian optimisation predicts an objective function and its probability distribution within a defined design space. This iterative approach balances exploitation, using data from the surrogate model, and exploration, searching unexplored areas, to efficiently uncover global optima. Each iteration refines the surrogate model's accuracy by incorporating new experimental data, enabling progressively better predictions. In the context of designing DFMs for integrated CO_2 capture and hydrogenation, Bayesian optimisation has not been used before, however, in the catalysts' design for CO_2 hydrogenation and other processes, it is demonstrated significant utility in reducing the number of experiments required to achieve optimal results, thereby controlling costs and project duration.[37–39]

In this paper, we synthesised 15%Ni1%Ru, *X*%Na/Ce–Al (where X = 2.5–15 wt%) DFMs, starting with a screening of 4 initial compositions to investigate the effect of adsorbent loading on the CO_2 capture and methanation process. The combination of Ni and Ru in CO_2 conversion catalysts has gained significant attention due to the synergistic effects that enhance catalytic performance.[40–46] Ru is known to improve the activity of Ni-based catalysts by increasing the dispersion and reducibility of Ni sites. Furthermore, the incorporation of Ni into Ru-based catalysts offers a cost-effective strategy by reducing the overall Ru loading while maintaining high catalytic activity.[47–50] This balanced combination of Ni and Ru (with the 10–20% ratios) not only optimises performance but also reduces material costs, making it a promising approach for sustainable CO_2 hydrogenation. This combination was kept constant for all samples as the goal was to perform some experiments, varying only the adsorbent loading, for the foundation of a basic model for optimisation study. We then used Bayesian optimisation to identify additional experiments to find the optimum adsorbent composition while reducing the number of the required experiments. Hence, the main goal of the study is the optimisation of the adsorbent loading for the NiRu*X*Na-DFMs utilising GP + BO. After acquiring data from experimental tests, we added the data to our GP model to be optimised by BO. The recommended point by the model was tested experimentally and the results were added to the model to get the next recommended point. We also thoroughly characterised the DFMs using XRD, SEM, EDS, BET, ICP-MS, CO_2-TPD, to understand how structural differences contribute to the observed methanation activity.

2 Results and discussion

All *X*Na-DFMs exhibited characteristic peaks corresponding to the support (γ-Al_2O_3, CeO_2) and to NiO which indicated the decomposition of Ni nitrates (Fig. 1) diffraction planes to Na_2O were observed in all samples.[51] Residual sodium nitrate peaks were evident in the XRD patterns, which increased while increasing the loading of sodium in samples. Peaks of RuO_2 were not observable in any *X*Na-DFM diffraction pattern as the amount is very low and they are probably present as dispersed nanoparticles on the support. The reference XRD patterns are presented in the ESI.†

SEM and EDS were performed for the lowest (2.5%) and the highest (15%) adsorbent loading DFMs. SEM and EDS mapping of 15Na-DFM (Fig. 2 and 3) indicate that Ni, Ru, Al, and Ce components are dispersed finely on the support. Areas rich in sodium were observed. Interpreting these results together with XRD results can identify these Na-rich regions as residual sodium nitrates from the sodium precursor. Additionally, the EDS mapping for 2.5Na-DFM, Fig. 4, demonstrated that at low sodium loading, these Na-rich areas appear to be less prevalent, which shows the better dispersion of the adsorbent and lower residual nitrates for lower loadings of the adsorbent.

Despite the observation of Na-rich regions on the surface of the DFMs, BET analysis (Table 1) indicates that the surface area and pore volume are influenced by the adsorbent loading, showing the preferential deposition of adsorbent in the pores of the support.

ICP-MS results for samples, Table 2, show that the loadings of the adsorbent (Na) and catalytic materials (Ni and Ru) are lower than the amounts described in ESI.† This would be due to the loss of some materials and not impregnating them on the support while weighing, mixing, or drying. However, the findings show almost the same loadings of Ni and Ru for all samples and an increasing trend for Na. The DFMs' nomenclature is based on the initial calculated amounts throughout the paper.

To evaluate the impact of adsorbent loading on the available weak (40–200 °C), medium (200–600 °C), and strong (>600 °C) basic sites (relevant for understanding differences in CO_2 capture behaviour) of the DFMs with different Na loadings, CO_2-TPD was performed. The results shown in Fig. 5 and Table 3 indicate that except for 2.5Na-DFM, the samples present weak, medium, and strong basic sites. However, as Table 3 shows, the amount of weakly, medium, and strongly adsorbed carbonates varies with the loading of the adsorbent. Table 3 shows increasing trends for medium and strong basic sites by increasing the Na-loading. More CO_2 desorption from medium basic sites with increasing Na-loading is an indicator that more CO_2 can be reversibly adsorbed at

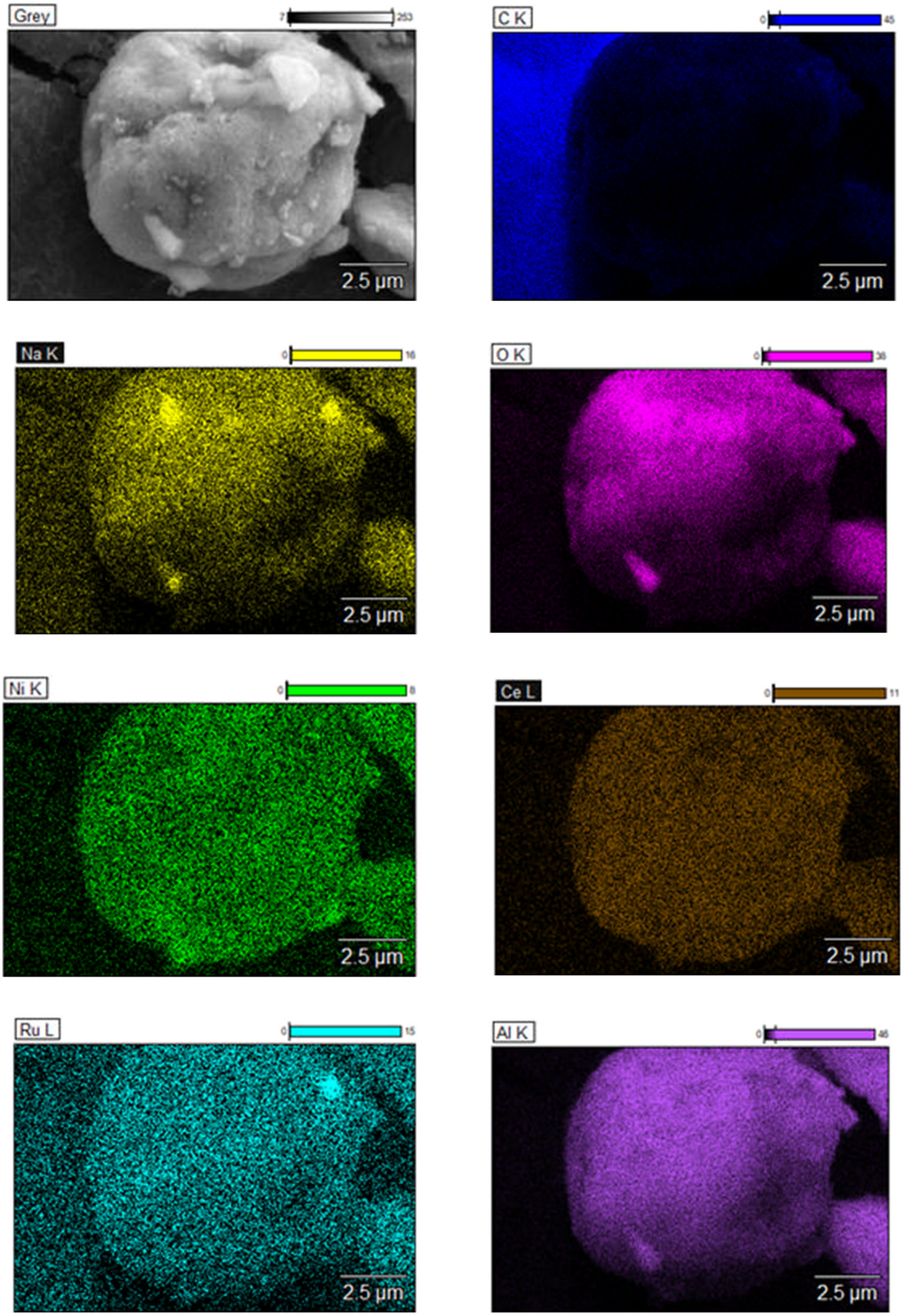

Fig. 4 EDS mapping of 15Ni1Ru, 2.5Na-DFM.

intermediate temperatures (relevant to catalysis). Since the focus of this study was CO_2 capture and methanation and the medium basic sites play a significant role at 400 °C, DFMs with higher loadings of sodium seem promising samples, with 15Na-DFM showing the highest number of medium basic sites. However, the highest CO_2 adsorption amount is not necessarily going to lead to the best performance of the DFM since the methanation performance depends on the reversibility of the CO_2 capture at temperatures where the catalyst is most active and also on the proximity and cooperation between adsorbent and catalyst sites. As per usual in catalysis

Table 1 Structural properties of 15Ni1RuXNa-DFMs (X = 2.5–15%)

DFMs	S_{BET} (m^2 g^{-1})	V_{pore} (cm^3 g^{-1})	D_{pore} (Å)
2.5Na-DFM	157	0.40	79
5Na-DFM	88	0.24	73
10Na-DFM	64	0.18	73
15Na-DFM	33	0.09	74

Table 2 Elemental loadings of 15Ni1RuXNa-DFMs (X = 2.5–15%)

DFMs	wt% Ni	wt% Ru	wt% Na
2.5Na-DFM	11.49	0.40	1.05
5Na-DFM	11.49	0.50	3.84
10Na-DFM	11.27	0.54	6.77
15Na-DFM	11.67	0.42	9.32

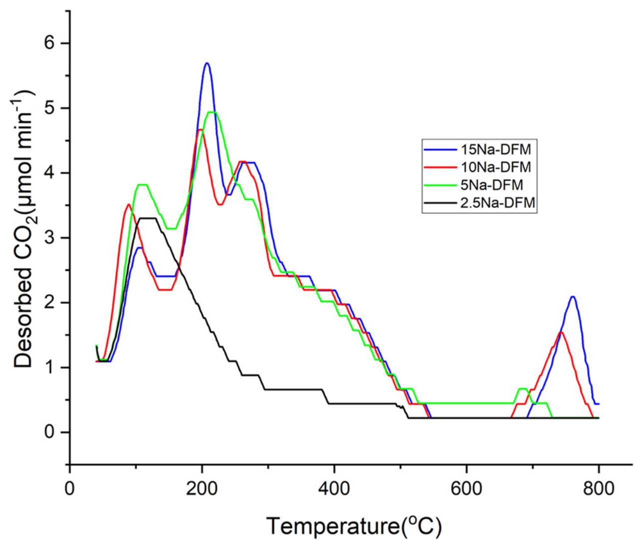

Fig. 5 CO_2-TPD profiles of 15Ni1Ru, XNa-DFMs (X = 2.5–15%), with 10% CO_2/N_2 (50 mL min^{-1}), 40–800 °C.

Table 3 Weak, medium, and strong basic sites 15Ni1RuXNa-DFMs (X = 2.5–15%)

DFMs	Desorbed CO_2 (µmol g_{DFM}^{-1}) Weak	Medium	Strong	Total
2.5Na-DFM	85.48	48.72	0	134.2
5Na-DFM	110.68	192.96	21.52	325.16
10Na-DFM	92.44	195.12	33.32	320.88
15Na-DFM	73.92	230.16	41.16	345.24

Sabatier's principle must be considered and the interplay of adsorption/reaction/desorption must be carefully adjusted.

H_2-TPSR has been performed for all XNa-DFMs after being exposed to air to evaluate the appropriate temperature for CO_2 methanation. The results of the dynamic evolution of gases are depicted in Fig. S1† and the H_2 consumption, CH_4, and CO production during the whole process (room temperature to 900 °C) are illustrated in Fig. 6. Fig. S1† demonstrates that for all samples the onset of H_2 consumption is before the CH_4/CO production, associated with the reduction of Ru and Ni metals to their active phase for the conversion of the adsorbed CO_2.[24,52,53] All samples except for 2.5Na-DFM produce both CH_4 and CO from the CO_2 captured from air with CH_4 being the main product at intermediate temperatures (350–600 °C). Moreover, all samples, except for 2.5Na-DFM, demonstrated that they have adsorbed CO_2 from the surrounding air prior to the test, indicating their potential use for direct air capture (DAC) processes.[26,31,54] Fig. 6, illustrating the quantitative analysis of H_2-TPSR tests, shows that increasing the adsorbent loading leads to enhanced CH_4 production until a Na loading of 5%. After this point, increasing the loading to 10 and 15% resulted in decreased overall production of CH_4. However, the increased H_2 consumption (2.7–10.1 mmol g_{DFM}^{-1}) with increased loading of adsorbent (2.5–15%), while the amount of Ni and Ru is same for all samples and decrease of CH_4 (167.86–62.5 µmol g_{DFM}^{-1}) and CO production (41.07–33.93 µmol g_{DFM}^{-1}) for 5–15% loadings, demonstrates that hydrogen is being consumed in other reaction(s) besides reducing the metals and producing CH_4 and CO. According to our previous study, this hydrogen consumption might be related to the conversion of Na_2O to sodium hydroxide (eqn (1)).[31,55]

$$Na_2O + H_2O \leftrightharpoons 2NaOH \quad (1)$$

The cyclic performance of XNa-DFMs was investigated for CO_2 adsorption and conversion processes at 400 °C, with described pre-treatment conditions in section 4. First, CO_2 adsorption was done at room temperature to saturate the DFM, after heating to 400 °C in 10% H_2/N_2 and holding at 400 °C to convert the adsorbed CO_2 to CH_4/CO, the cyclic adsorption/hydrogenation tests were performed for four cycles. The dynamic results are demonstrated in Fig. S2,† and

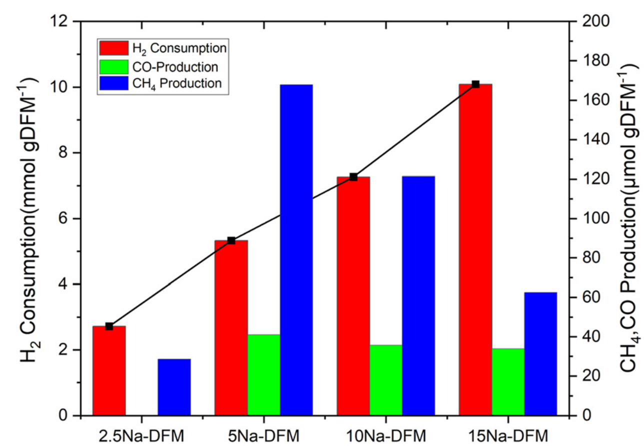

Fig. 6 Total H_2 consumption, CH_4 production and CO production of 15Ni1Ru, XNa-DFMs (X = 2.5–15%) during H_2-TPSR, with 10% H_2/N_2 (50 mL min^{-1}), 25–900 °C.

CH_4, and CO produced during adsorption and hydrogenation are depicted in Fig. 7–9. Dynamic activity plots (Fig. S2†) show that all the *X*Na-DFMs have almost the same capture and conversion performance over four cycles, which indicates that no obvious material degradation occurs after the first cycle, although it should be noted that long term aging studies (including real emission streams) are needed to determine the suitability of any DFM for industrial implementation. All samples demonstrate some CO production during adsorption, which shows that pre-reduction of some metallic sites available on the surface contributes to CO_2 dissociation. CO production during capture is the highest for the 2.5Na-DFM and it decreases as the loading of sodium increases (Fig. 7). This could be related to the enhancement in reducibility of NiRu in the presence of low loading of Na, as the reduction peaks shift to lower temperatures by the addition of Na to Ni and Ru catalysts.[30,56–58] Fig. S1† also demonstrates that the onset of H_2 consumption shifts to higher temperatures by increasing Na-loading. Fig. 8 and 9 illustrate that the CH_4 and CO productions during hydrogenation follow the same trend, except for 15Na-DFM. By increasing the loading of sodium up to 10% both CH_4 and CO production increase, a further increase to 15% Na, results in a drop in CH_4 and CO production. These findings reveal that, probably, the blockage of the pores, reduced surface area, and coverage of NiRu sites as shown by SEM/EDS are responsible for the lower CO_2 methanation performance of 15Na-DFM despite its better CO_2 desorption during CO_2-TPD at medium temperatures. The total amounts of CH_4 and CO produced during adsorption and hydrogenation (in 4 cycles) show that the highest CH_4 produced belongs to 10Na-DFM with 391.07 μmol g^{-1} in the first cycle. The produced gases during H_2-TPSR and first and last cycles are exhibited in Table 4. The methane and CO productions show that despite the 10Na-DFM showing the highest CH_4 production, its selectivity towards methane is the lowest (89.14%) due to the higher CO produced in hydrogenation. Selectivity decreases in the order 2.5Na-DFM > 15Na-DFM > 5Na-DFM >10Na-DFM (Table 5). NiRu's selectivity towards methane production can change by adding Na to the catalyst. RWGS could occur at lower temperatures over NiRuNa DFMs due to the partially reduced oxides of NiRu.[59–61]

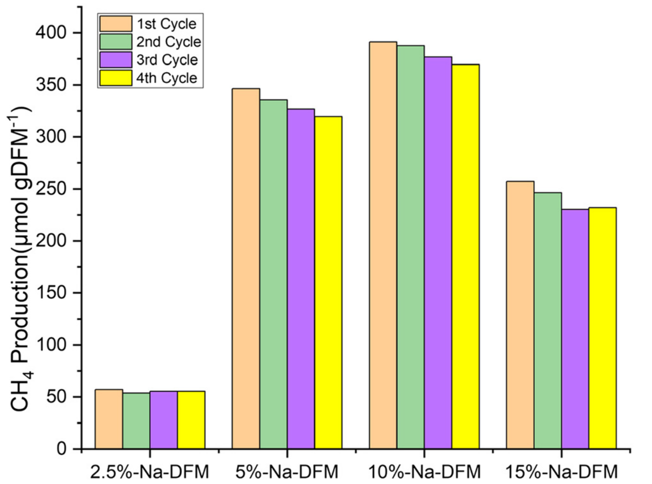

Fig. 8 CH_4 production during the hydrogenation step for 15Ni1Ru, *X*Na-DFMs (*X* = 2.5–15%), at 400 °C, with $10H_2/N_2$ (50 mL min^{-1}) in hydrogenation step – 15 minutes.

The findings from characterisation and activity screening tests show that the DFM's performance is not continuously improved by the addition of more adsorbent during synthesis but shows an interplay of multiple effects. The increase in Na loading leads to differences in the formation of Na oxide due to changes in the precursor reducibility (due to agglomeration) and resulting dispersion on the support, with some Na covering NiRu nanoparticles. Moreover, the activity screening results imply that Na loading also influences NiRu

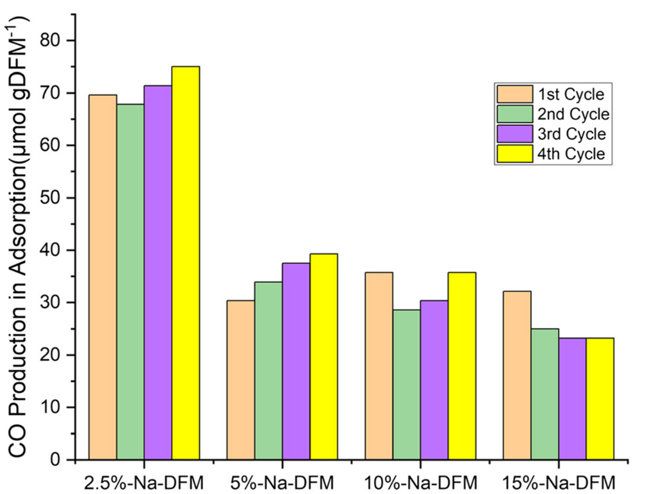

Fig. 7 CO production during the adsorption step for 15Ni1Ru, *X*Na-DFMs (*X* = 2.5–15%), at 400 °C, with 10% CO_2/N_2 (50 mL min^{-1}) in adsorption step – 15 minutes.

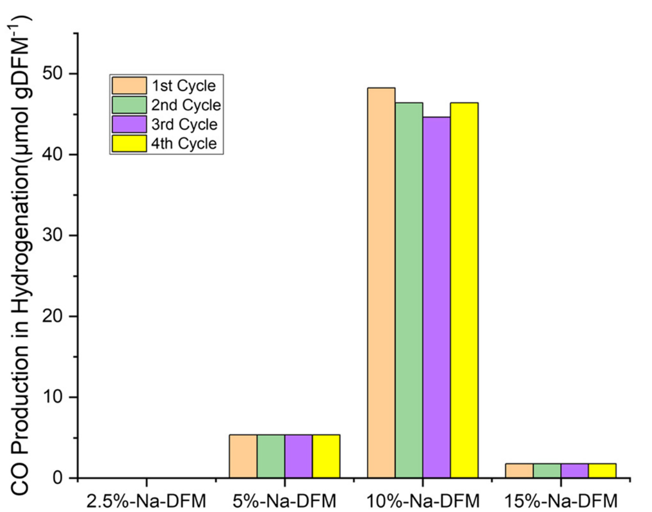

Fig. 9 CO production during the hydrogenation step 15Ni1Ru, *X*Na-DFMs (*X* = 2.5–15%), at 400 °C, with $10H_2/N_2$ (50 mL min^{-1}) in hydrogenation step – 15 minutes.

Table 4 Gases produced during H_2-TPSR, first and last cycle

	Produced gases (μmol g_{DFM}^{-1})							
DFM	CH_4-TPSR	CO-TPSR	CH_4-Cycle 1	CH_4-Cycle 4	CO-Hyd-Cycle 1	CO-Hyd-Cycle 4	CO-Ads-Cycle 1	CO-Ads-Cycle 4
2.5Na-DFM	132.14	0.00	57.14	55.36	0.00	0.00	69.64	75.00
5Na-DFM	337.50	7.14	346.43	319.64	5.36	5.36	30.36	39.29
10Na-DFM	214.29	5.36	391.07	369.64	48.21	46.43	35.71	35.71
15Na-DFM	189.26	7.14	257.14	232.14	1.79	1.79	32.14	23.21

Table 5 Average methane production and selectivity of 15Ni1Ru, *X*Na-DFMs (*X* = 2.5–15%)

DFMs	Average methane produced in 1 cycle (μmol g_{DFM}^{-1})	Average selectivity (%)
2.5Na-DFM	55.36	100.00
5Na-DFM	332.14	98.41
7.9Na-DFM	398.60	96.04
10Na-DFM	381.25	89.14
15Na-DFM	241.52	99.26

reducibility and hence low Na loadings can promote undesirable CO production during adsorption, while higher loadings can lower the selectivity to methane. The results from CO_2-TPD tests illustrate that by increasing the loading of the adsorbent, the medium basic sites to capture CO_2 increase while the H_2-TPSR results indicate that the catalytic material should also be sufficiently available on a higher surface area to convert this adsorbed CO_2. 15Na-DFM did not possess the highest CH_4/CO production while it had the highest CO_2 desorbed during CO_2-TPD test. An interesting result was that the sample with 5% Na-loading, showed the highest CH_4 production during H_2-TPSR (CO_2 was adsorbed directly from the air before the experiment started), while it did not produce the highest methane during isothermal cyclic tests (conversion time 20 minutes and conversion temperature 400 °C with 10% CO_2/N_2.) These findings illustrate the convoluted nature of material optimisation due to the interdependency of catalyst activity and adsorbent–catalyst interaction and show that clearly we cannot find the true optimum composition in an initial screening study. This is where computational techniques can be of use for material optimisation with fewer numbers of experiments.

The GP models for both selectivity towards methane and produced methane were developed using the initial screening results and are illustrated in Fig. S3 and S4.† The models showed the areas with uncertainty indicate the possible loadings of Na with higher produced methane and selectivity. BO recommended 7.9% of Na-loading as the next point to explore. The results of the cyclic test for this sample with the same conditions described in section 4 are demonstrated in Fig. S5† and Table 5.

The cyclic activity results for the 7.9Na-DFM (recommended by the Bayesian optimisation), show that this sample demonstrated stable performance during three cycles, the produced methane is the highest for this sample, and the selectivity is better than the 10Na-DFM (Table 5). This indicates that the GP model and optimisation are reliable, and it can recommend samples with higher methane production and good selectivity. The data from the cyclic test of 7.9Na-DFM was also added to the model. Fig. 10 and 11 illustrate the predictions of the models after adding 7.9% in *X* and the regarding selectivity and produced methane in Y_1 and Y_2 datasets, respectively.

The subsequent recommended point was 6.7% for Na-loading with predicted Y_1 = 90.67% and predicted Y_2 = 380.94 μmol g_{DFM}^{-1}. Since the loading amount (*X*) is very close to the previous loading (1.2% difference) and selectivity and produced methane do not show much difference with the previous point, a plateau was forming, 7.9Na-DFM was selected as the DFM with optimal loading of Na.

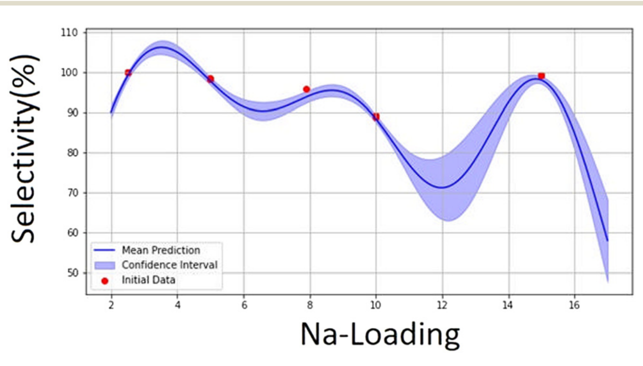

Fig. 10 Selectivity towards methane predicted by BO utilising GP model for 15Ni1Ru, *X*Na-DFMs (*X* = 2.5–15%).

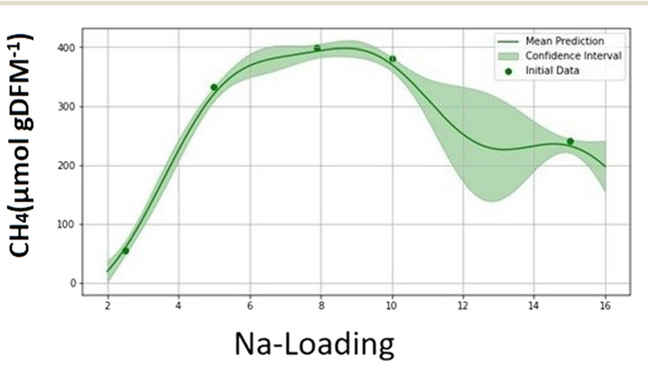

Fig. 11 Produced methane predicted by BO utilising GP model for 15Ni1Ru, *X*Na-DFMs (*X* = 2.5–15%).

The results for the realistic testing (Fig. 12 and 13) show that the presence of oxygen and water can affect the performance of the 7.9Na-DFM in CO_2 capture and methanation processes. As the dynamic curves (Fig. 12) demonstrate, "A" for adsorption step and "H" for hydrogenation step, the onset of methane production in the catalytic conversion step was delayed and decreased when O_2 and H_2O were present in the adsorption step. This may be associated with the impact of O_2 on the catalytic materials, especially Ni.[27,62,63] Oxygen can oxidise the metallic sites, which deactivates them for methanation. However, Ru can facilitate the reducibility of Ni during hydrogenation.[35,46,64] During the hydrogenation step, first, the oxidised metals are reduced to their active forms, and then these reduced sites can catalyse the methanation reaction. Due to this delay, the methane peak is not as sharp as in ideal conditions but broader. The cycles where O_2 and H_2O were present during the capture step (C2–6 inclusive in Fig. 13b) also show increasing amounts of desorbed CO_2 during hydrogenation; this CO_2 desorption is associated with the delay for the reduction of the metallic sites that can lead to lower methane production since the desorbed CO_2 cannot spill over to adjacent catalytic sites at the beginning of the conversion step, and they will leave the reactor unreacted.[25,41] In addition, the selectivity during hydrogenation shifts slightly towards CO production under realistic conditions (methane selectivity goes from 98.8% to 97.7% for C1 and C2, and 94.7% for C3 to 86.6% for C6) due to the presence of partially oxidised sites and probably because of the competition between methanation and moisture-driven desorption of adsorbed carbonates.[35,61] The selectivity to methane increased again when oxygen and water were no longer present in the feed gas (C7 and C8 to 95.5% and 97.7%, respectively). It should be noted that due to the shorter cycle time used in this test, the tail end of methanation activity for cycles C2–6 inclusive was cut off, which also contributed slightly to the lowered methanation activity measurements. After switching back to O_2-free and dry conditions (C7, C8), the DFM regains its original capture and conversion capability, indicating reversible deactivation through oxidation during the realistic testing. Another interesting finding was associated with the production of CO during adsorption due to the presence of reduced sites (which dissociate CO_2). When oxygen was present in the feed gas, undesirable CO formation was completely suppressed (Fig. 13a), as oxygen oxidised the reduced metallic sites.[62] All in all, the results demonstrate that the presence of O_2 and H_2O benefits CO_2 capture by suppressing CO formation but slows down methanation, leading to increased CO_2 desorption and lower methanation activity (36% decrease in produced methane). However, the DFM showed stable performance for realistic cycles, and it regained nearly all its original methanation capacity after the elimination of O_2 and H_2O from the feed gas. This behaviour is associated with the dynamic (oxidising/reducing) nature of the adsorption–conversion cycles.

3 Conclusions

Na adsorbent loading on NiRuNa DFMs has been optimised using a combination of experimental activity screening and Bayesian Optimisation. The findings from

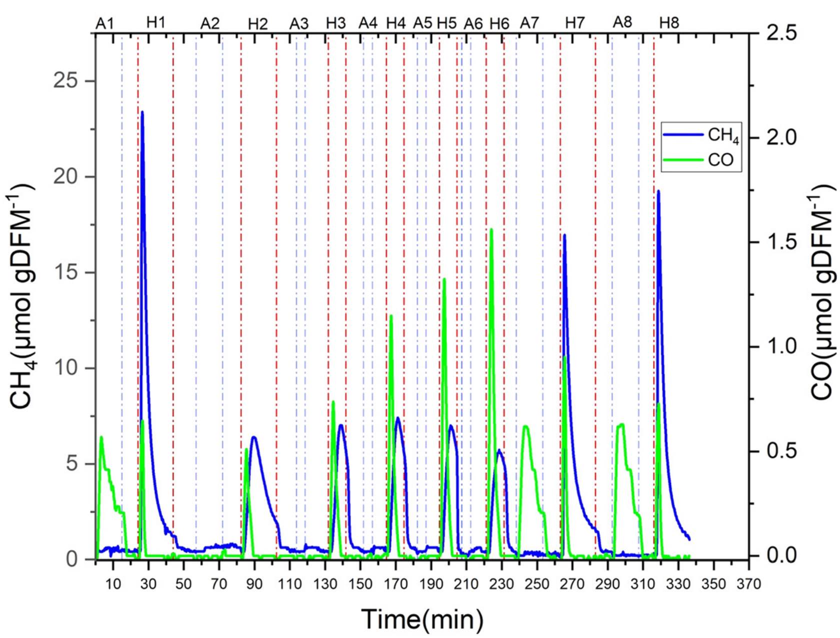

Fig. 12 Dynamic curves of ideal and realistic cyclic testing with 15Ni1Ru, 7.9Na/Al, ideal adsorption step: 10% CO_2/N_2, realistic adsorption step: 10%CO_2 + 2.7%O_2 + 2.9%H_2O/Ar, hydrogenation step: 10% H_2/N_2, at 400 °C.

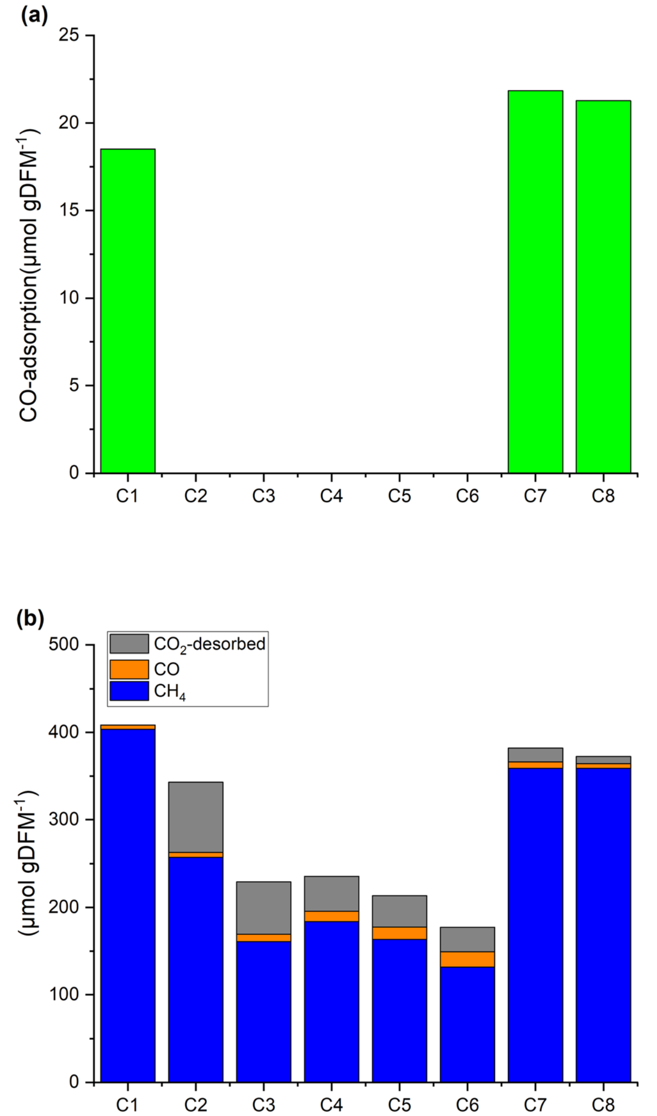

Fig. 13 Produced gases during hydrogenation in ideal and realistic cyclic testing with 15Ni1Ru, 7.9Na/Al, ideal adsorption step: 10% CO_2/N_2, realistic adsorption step: 10%CO_2 + 2.7%O_2 + 2.9%H_2O/Ar, hydrogenation step: 10% H_2/N_2, at 400 °C.

H_2-TPSR and cyclic activity showed that the addition of Na to NiRu can affect performance not just *via* increased number of adsorption sites for CO_2 but can also influence the selectivity of the catalytic sites, an effect we have ascribed to a change in NiRu reducibility. The availability of reduced metallic sites could lead to different results during adsorption and hydrogenation steps. The reduced metallic sites could contribute to CO production during adsorption, while their presence in sufficient numbers could lead to higher CH_4 production during hydrogenation. Partially reduced NiRu sites could shift the selectivity towards CO production during hydrogenation. The CO_2-TPD results indicated that the highest CO_2 capture capability will not necessarily lead to the highest methanation capacity. All of these results emphasised that an optimisation approach is required to find out the optimal loading. Bayesian optimisation with Gaussian process utilised in this study offers a novel approach to finding the true optimal adsorbent loading of DFMs. While the model herein focused only on adsorbent loading optimisation, it can be a starting point for overall composition optimisation in DFMs where new combinations of adsorbent and catalyst are being tested. The best performing DFM, which was recommended by the BO and GP, with a loading of 7.9% Na demonstrated a methane production capacity per cycle of 398.6 μmol g_{DFM}^{-1} with good selectivity (96.04%). The realistic testing with 7.9Na-DFM showed that the presence of O_2 and H_2O favourably affects the capture stage by suppressing CO formation, but results in slower methanation performance of the DFM, however, this impact is reversible. By increasing the hydrogenation time and the concentration of H_2 during hydrogenation, the DFM could show a stable performance under real conditions.

This study is limited to a simplified (idealised) feed to develop the GP + BO model at a certain temperature. For the foundation of this model, a feed gas composition of 10% CO_2/N_2 was selected, as it closely reflects the concentration of CO_2 in most industrial point sources.[8,65] The focus was placed on adsorbent loading, representing an initial step toward employing computational tools in material design for ICCU. Several limitations were encountered in implementing this novel approach. Notably, the effects of O_2 and steam were not evaluated while performing the optimisation tests, despite their presence in typical industrial waste streams, and the stability tests were not applied. Nevertheless, the proposed model and methodology can be adapted for various setups using different process parameters, with different feed gas compositions, enabling the investigation of both adsorbent and catalytic material compositions in DFMs.

4 Experimental

The synthesis method followed a similar protocol to our previous work.[31] Briefly, DFMs were synthesised using sequential wet impregnation. First, the adsorbent was impregnated on the support through dissolution. For various loadings of Na, the calculated amounts of sodium precursor, $NaNO_3$ (Fluka), were dissolved in deionised water and the support CeO_2(20)–Al_2O_3(80), (SCFa-160 Ce20 Puralox), was added to the solution. Each loading for Na precursor was calculated as described in ESI.† After stirring the mixture with a magnetic stirrer for 30 minutes at room temperature, the mixture was transferred to a rotary evaporator flask to remove the excess water at elevated temperature and reduced pressure (60–70 °C, atmospheric pressure to 100 mbar). The obtained powder was placed in the oven at 120 °C overnight to complete the drying procedure. After that, the dried sample was transferred to a muffle furnace and calcined at 400 °C for 4 hours (with a 5 °C min^{-1} heating ramp). During this calcination step sodium nitrate was thermally decomposed to the dispersed oxides by following eqn (2) and (3).[66]

$$NaNO_3 \rightarrow NaNO_2 + O_2 \tag{2}$$

$$2NaNO_2 \rightarrow N_2O + \frac{3}{2}O_2 + N_2 \tag{3}$$

The data from XRD spectra and XPS (our previous work[31]) can confirm the presence of Na_2O, which can turn to NaOH in the presence of water (from the air).

Once the supported adsorbents, namely 2.5% Na/CeO_2–Al_2O_3, 5% Na/CeO_2–Al_2O_3, 10% Na/CeO_2–Al_2O_3, and 15% Na/CeO_2–Al_2O_3 were formed, the second phase of synthesis began. In the second stage of synthesis, the calculated quantities of catalyst precursors, as described in the ESI,† $Ni(NO_3)_2·6H_2O$ (Acros Organics), and $Ru(NO)(NO_3)_3$ solution (1.5 w/v Ru, Alfa Aesar), were dissolved in deionised water and the supported adsorbents with various loadings of sodium were added to the solution, separately, to achieve the final 15Ni1Ru–*X*Na/CeO_2–Al_2O_3 (X = 2.5, 5, 10 and 15) DFMs. The weight percentages of the adsorbent after impregnation of the catalytic materials became 2.2%, 4.3%, 8.6%, and 12.9%. Following the same steps as stage 1 for supported adsorbents, the excess water of DFMs was removed by drying in the oven before calcination at 500 °C (5 °C min^{-1}) for 3 hours in a muffle furnace. The sample recommended by the Bayesian optimisation (15Ni1Ru–7.9Na/CeO_2–Al_2O_3) was also synthesised following the same procedure. For simplicity, the DFMs were named 2.5Na-DFM, 5Na-DFM, 7.9Na-DFM, 10Na-DFM, and 15Na-DFM in this article. The exact loadings of sodium are characterised by the ICP-MS method. The safety precautions described in ESI.†

X-ray diffraction (XRD) was conducted for all *X*Na-DFMs (X = 2.5, 5, 10, 15) to evaluate the crystalline phase utilising the X'Pert Powder apparatus from PANalytical. Cu Kα radiation was used, with a wavelength of λ = 0.154 nm. The diffraction patterns were recorded over a $2\theta°$ range of 10–90° at 30 mA and 40 kV.

Elemental mapping was achieved by employing scanning electron microscopy (SEM) and energy dispersive spectroscopy (EDS) techniques. EDS analysis was conducted by a JEOL JSM-7100F instrument. Pathfinder software was used to perform the mappings. Moreover, the microscopic image of 15Na-DFM was obtained using the same device. Carbon paint was used to fix the DFMs to the holder, and to decrease the charging effect, silver paint and gold coating were applied.

The porosity and surface area of the samples were analysed by the Brunauer–Emmett–Teller (BET) method using a Micromeritics 3Flex apparatus. DFMs were initially degassed in a vacuum at 150 °C for 2 hours before obtaining the N_2 adsorption–desorption isotherms at liquid nitrogen temperature (−196.15 °C).

Gases (99.80% CO_2, 99.998% N_2) coming from cylinders (Linde) were used to feed a 10% CO_2/N_2 mixture when performing all the tests. As Table 1 in our review paper[8,65] shows, there are point sources with almost 10% CO_2 in their waste stream such as waste incineration smoke, coal burning, and IGCC smoke. Hence, considering 10% CO_2/N_2 as feed gas can reflect the concentrations that are available in several point sources.

To evaluate the basicity of the surface of the *X*Na-DFMs temperature programmed desorption (CO_2-TPD) was employed. TPD profiles were obtained using a fixed-bed quartz reactor (0.4″ ID) housed in a tube furnace. 250 mg of DFM was placed in the reactor and the temperature was fixed at 40 °C, then a 50 mL min^{-1} 10% CO_2/N_2 mixture was introduced to the reactor for 45 minutes. After purging with N_2 for 30 minutes, the temperature was increased from 40 to 800 °C with a 10 °C min^{-1} ramp to achieve CO_2 desorption. The vol% of CO_2 was recorded every 5 seconds using an online ABB AO2020 analyser with a sensitivity of 0.01%.

The elemental composition of the DFMs was determined by ICP-MS using an iCAP 7200 ICP-OES Duo spectrometer (Thermo Fisher Scientific) and solutions of the DFMs with a concentration of 10 mg 30 mL^{-1} in all cases. The solutions were prepared by microwave acid digestion (HCl : HNO_3 1 : 1) in an ETHOS EASY microwave digestion platform (Milestone) at 230 °C for 15 min. The content of the Ni, Ru and Na were analysed by this method.

Temperature programmed reduction was performed on DFMs which had been exposed to air after synthesis. As these samples have adsorbed CO_2 from the ambient environment, leading to reactions with hydrogen, we are referring to these tests as temperature programmed surface reactions with hydrogen (H_2-TPSR). In this approach, 250 mg of DFM was loaded in the fixed-bed quartz reactor with 0.4″ ID. Subsequently, 10% of H_2/N_2 (50 mL min^{-1}) was introduced to the reactor while the temperature was ramped from room temperature to 900 °C (10 °C min^{-1}). CH_4, CO, CO_2, and H_2 were detected using an online ABB AO2020 analyser equipped with IR and TCD detectors.

Cyclic tests for CO_2 capture and hydrogenation were performed to evaluate the *X*Na-DFMs, to investigate their adsorption and conversion activity through four consecutive cycles. The fixed quartz bed reactor with 0.4″ ID was used for these tests. 250 mg of the DFM was loaded into the reactor. 50 mL min^{-1} 10% CO_2/N_2 was sent to the reactor for 30 minutes at room temperature to saturate the sample, after 10 minutes of purge with N_2, the samples were heated to 400 °C in hydrogen – using a 50 mL min^{-1} feed of 10% H_2/N_2. The samples were held at 400 °C in the hydrogen mixture until methane production could no longer be detected. This has been done to ensure that the surface is clean from carbonates and the sample is ready for cyclic test. Subsequently, holding the temperature at 400 °C, 50 mL min^{-1} 10% CO_2/N_2 was introduced into the reactor during the "CO_2 capture" step (15 min). The reactor was then purged with N_2 to prevent gas phase mixing of CO_2 and H_2 so that all carbon containing products could be attributed to adsorbed CO_2. In the conversion step, 50 mL min^{-1} 10% H_2/

N_2 was fed to the reactor for 20 minutes to convert the adsorbed CO_2 to hydrogenation products. At the end of each cycle of adsorption and hydrogenation, an N_2 purge was utilised to purge all the H_2 and get the setup ready for the next cycle. Vol% of the feed gases and products (CO_2, H_2 CH_4, and CO) was recorded by the online ABB AO2020 analyser.

The realistic testing is done following the same procedure for cyclic tests, with 7.9Na-DFM. For these experiments, first, CO_2 adsorption was completed at room temperature (for 30 min) and after heating to 400 °C in the presence of 10% H_2/N_2 and keeping it there until CH_4 reached zero, the cyclic tests started. The first cycle (C1), was the ideal testing of the sample for comparison purposes with 10% CO_2/N_2 (50 mL min^{-1}) for 15 min during the capture step and 10% H_2/N_2 (50 mL min^{-1}) during the hydrogenation step for 20 min. The second cycle (C2) followed the same steps with 10%CO_2 + 2.7%O_2 + 2.9%H_2O/Ar (50 mL min^{-1}) during adsorption and 10% H_2/N_2 (50 mL min^{-1}) for methanation to assess the behaviour of the sample under realistic conditions. O_2 was sent into the reactor from a cylinder containing 3%O_2 + 97%Ar, and the feed gas passed through a water bubbler before entering the reactor. Cycles three to six (C3–C6) were done under the same realistic conditions except for the adsorption and hydrogenation time, which were 5 and 10 min, respectively. These durations are chosen to have more cycles in a certain period. Cycles seven and eight (C7 and C8) were done under ideal conditions (10% CO_2/N_2 for 15 min and 10% H_2/N_2, for 20 min, 50 mL min^{-1} total flow rate) after realistic conditions to evaluate the regaining of the capture and methanation capability of the sample when oxygen and water were no longer present in the feed gas. The online ABB analyser recorded the gas composition (CO_2, CO, CH_4, and H_2) every 5 seconds.

We used Bayesian optimisation (BO) with a Gaussian process (GP) surrogate to find the optimal loading for NiRu, XNa (X: 2.5–15% wt) DFMs, using the data from our initial screening studies, produced methane and selectivity for 4 different loadings of sodium in 4 cyclic adsorption (10% CO_2/N_2) hydrogenation (10% H_2/N_2) tests at 400 °C. The GPyOpt package was used in this optimisation.[67] The loading of the sodium was the initial input $X \in [2, 16]$, and the selectivity towards methane and the average produced methane over four cycles for each loading were the objectives (Y_1 and Y_2, respectively). Since the significance of the two objectives was the same, the final objective was written as:

$$Y = w_1Y_1 + w_2Y_2 \tag{4}$$

The initial dataset (4 points) forms the initial training set for the Gaussian process (GP) models, which are trained to predict objective values at unexplored points in the domain. The GP surrogate was selected due to its suitability for handling sparse data and providing uncertainty estimates at predicted points. Separate GP models were constructed for each objective, allowing for flexible and independent modelling. The RBF (radial basis function) kernel was utilised for both (Y_1 and Y_2) models because of its smoothness properties and capability to capture variations in the objective functions across the domain. To ensure the GP models interpolated the initial data exactly, the noise variance parameter in each model was fixed to 0.2. After producing a surrogate model with the aid of GP, Bayesian optimisation was applied to iteratively explore the domain, identifying the next best experimental input (X: Na loading) that maximises the produced methane and selectivity towards methane simultaneously. The expected improvement (EI) acquisition function was used to balance exploration and exploitation.

Data availability

Data for this article, including the X–Y data for Fig. 5, 7–10, S1, S2 and S5† is available at Mendeley Data Repository at DOI: **https://doi.org/10.17632/36j9dpfxjf.1**.

Conflicts of interest

The authors declare no conflict of interest.

Acknowledgements

The financial support for this study was provided by the Faculty of Physics and Engineering of the University of Surrey. The team at the University of Seville acknowledges support from the Spanish Ministry of Science through SMART-FTS project (ref: PID2021-126876OB-I00) and FPU grant (FPU21/04873). Sasol is kindly acknowledged for providing Al_2O_3–CeO_2 support. The technician team of the Chemical and Process Engineering department, Ben Gibbons, Matthew Crick and Yusuf El-Hassan, of the University of Surrey is greatly acknowledged for their technical support.

References

1 X. G. Zhang, A. Buthiyappan, N. Z. Mohd Azmi and A. A. Abdul Raman, Towards circular carbon economy: Recent developments and techno-economic assessment of integrated carbon dioxide capture and utilization, *Chem. Pap.*, 2024, **78**, 7729–7738.

2 J. Li, X. He and R. Hu, Integrated carbon dioxide capture and utilization for the production of CH_4, syngas and olefins over dual-function materials, *ChemCatChem*, 2024, **16**, e202301714.

3 Z. Lv, J. Han, T. Deng, C. Gao, J. Li and C. Qin, Study on the arrangement of CO_2 sorbent and catalyst for integrated CO_2 capture and methanation, *Sep. Purif. Technol.*, 2025, **355**, 129679.

4 J. Chen, Y. Xu, P. Liao, H. Wang and H. Zhou, Recent progress in integrated CO_2 capture and conversion process using dual function materials: A state-of-the-art review, *Carbon Capture Sci. Technol.*, 2022, **4**, 100052.

5 R. Ahmadov, S. S. Michtavy and M. D. Porosoff, Dual functional materials: At the interface of catalysis and separations, *J. Am. Chem. Soc.*, 2024, **40**, 123–130.
6 E. García-Bordejé and R. González-Olmos, Advances in process intensification of direct air CO_2 capture with chemical conversion, *Prog. Energy Combust. Sci.*, 2024, **100**, 101132.
7 Z. L. Guo, X. L. Bian, Y. B. Du, W. C. Zhang, D. D. Yao and H. P. Yang, Recent advances in integrated carbon dioxide capture and methanation technology, *J. Fuel Chem. Technol.*, 2023, **51**, 293–303.
8 S. B. Gharamaleki, T. R. Reina and M. S. Duyar, Taking dual function materials (DFM) from the laboratory to industrial applications: A review of DFM operation under realistic integrated CO_2 capture and utilization conditions, *Prog. Energy*, 2025, **7**, 012001.
9 M. C. Freyman, Z. Huang, D. Ravikumar, E. B. Duoss, Y. Li, S. E. Baker, S. H. Pang and J. A. Schaidle, Reactive CO_2 capture: A path forward for process integration in carbon management, *Joule*, 2023, **7**, 631–651.
10 M. Dolat, K. Keynejad, M. S. Duyar and M. Short, Superstructure optimisation of direct air capture integrated with synthetic natural gas production, *Appl. Energy*, 2025, **384**, 125413.
11 A. Shojaeinia, A. G. Poshtahani, S. O. Kia, A. Mashtizadeh, H. Aghajani and A. T. Tabrizi, A Review of advances in carbon dioxide capture with the aim of reusing them as fuel, *Univers. J. Carbon Res.*, 2024, **2**, 32–46.
12 A. Bhaskaran, S. A. Singh, B. M. Reddy and S. Roy, Integrated CO_2 capture and dry deforming of CH_4 to syngas: A review, *Langmuir*, 2024, **40**, 14766–14778.
13 B. Lu, Y. Fan, X. Zhi, Z. Han, F. Wu, X. Li, C. Luo and L. Zhang, Material design and prospect of dual-functional materials for integrated carbon dioxide capture and conversion, *Carbon Capture Sci. Technol.*, 2024, **12**, 100207.
14 X. Su and L. Shen, Advances and challenges about Ni-based dual functional materials for alternating cycles of CO_2 storage and in-situ hydrogenation to CH_4, *Carbon Capture Sci. Technol.*, 2024, **13**, 100278.
15 T. Tatsumichi, R. Okuno, H. Hashimoto, N. Namiki and Z. Maeno, Direct capture of low-concentration CO_2 and selective hydrogenation to CH_4 over Al_2O_3-supported Ni-La dual functional materials, *Green Chem.*, 2024, **26**, 10842–10850.
16 E. García-Bordejé, A. Belén Dongil, J. M. Conesa, A. Guerrero-Ruiz and I. Rodríguez-Ramos, Dual functional materials based on Ni and different alkaline metals on alumina for the cyclic stepwise CO_2 capture and methanation, *J. Chem. Eng.*, 2023, **472**, 144953.
17 C. Jeong-Potter, M. Abdallah, S. Kota and R. Farrauto, Enhancing the CO_2 adsorption capacity of γ-Al_2O_3 supported alkali and alkaline-earth metals: Impacts of dual function material (DFM) preparation methods, *Ind. Eng. Chem. Res.*, 2022, **61**, 10474–10482.
18 Z. K. Guo, S. Gao, S. X. Xiang, J. P. Wang, G. C. Mao, H. L. Jiang, B. X. Dong and Y. L. Teng, Mechanochemical synthesis of Ni/MgO dual functional materials at room temperature for CO_2 capture and methanation, *J. Chem. Eng.*, 2024, **481**, 148599.
19 J. Chu, C. Liang, W. Xue, P. Huang, Y. Guo, R. Wang, J. Sun, W. Li and C. Zhao, Revealing the effect of synthetic method on integrated CO_2 capture and conversion performance of Ni-Na_2ZrO_3 bifunctional materials, *Sep. Purif. Technol.*, 2024, **346**, 127534.
20 J. Marin, P. Parra and L. Rios, Improved Dual Function Materials for CO_2 Capture and in situ methanation, *Energy Technol.*, 2023, **12**, 00952.
21 J. A. Onrubia-Calvo, B. Pereda-Ayo, J. A. González-Marcos and J. R. González-Velasco, Lanthanum partial substitution by basic cations in $LaNiO_3/CeO_2$ precursors to raise DFM performance for integrated CO_2 capture and methanation, *J. CO2 Util.*, 2024, **81**, 102704.
22 C. Jeong-Potter, M. A. Arellano-Treviño, W. W. McNeary, A. J. Hill, D. A. Ruddy and A. T. To, Modified Cu–Zn–Al mixed oxide dual function materials enable reactive carbon capture to methanol, *EES Catal.*, 2024, **2**, 253–261.
23 A. Bermejo-López, B. Pereda-Ayo, J. A. Onrubia-Calvo, J. A. González-Marcos and J. R. González-Velasco, How the presence of O_2 and NO_x influences the alternate cycles of CO_2 adsorption and hydrogenation to CH_4 on Ru-Na-Ca/Al_2O_3 dual function material, *J. CO2 Util.*, 2023, **67**, 102343.
24 S. J. Park, M. P. Bukhovko and C. W. Jones, Integrated capture and conversion of CO_2 into methane using $NaNO_3$/MgO + Ru/Al_2O_3 as a catalytic sorbent, *J. Chem. Eng.*, 2021, **420**, 130369.
25 L. P. Merkouri, L. F. Bobadilla, J. L. Martín-Espejo, J. A. Odriozola, A. Penkova, G. Torres-Sempere, M. Short, T. R. Reina and M. S. Duyar, Integrated CO_2 capture and dynamic catalysis for CO_2 recycling in a microbrewery, *Appl. Catal., B*, 2025, **361**, 124610.
26 L. P. Merkouri, T. R. Reina and M. S. Duyar, Feasibility of switchable dual function materials as a flexible technology for CO_2 capture and utilisation and evidence of passive direct air capture, *Nanoscale*, 2022, **14**, 12620–12637.
27 Q. Zheng, R. Farrauto and A. C. Nguyen, Adsorption and methanation of flue gas CO_2 with dual functional catalytic materials: A parametric study, *Ind. Eng. Chem. Res.*, 2016, **55**, 6768–6776.
28 Y. Lin, M. J. Abdallah, J. E. Peters, T. Luo, H. Sheng, Y. L. Chen and R. J. Farrauto, Aging studies of dual functional materials for CO_2 direct air capture with in situ methanation under simulated ambient conditions, *J. Chem. Eng.*, 2024, **479**, 147495.
29 M. S. Duyar, M. A. A. Treviño and R. J. Farrauto, Dual function materials for CO_2 capture and conversion using renewable H_2, *Appl. Catal., B*, 2015, **168–169**, 370–376.
30 A. Bermejo-López, B. Pereda-Ayo, J. A. González-Marcos and J. R. González-Velasco, Mechanism of the CO_2 storage and in situ hydrogenation to CH_4. Temperature and adsorbent loading effects over Ru-CaO/Al_2O_3 and Ru-Na_2CO_3/Al_2O_3 catalysts, *Appl. Catal., B*, 2019, **256**, 117845.

31 S. B. Gharamaleki, S. C. Ruiz, A. Penkova, T. R. Reina and M. I. S. Duyar, Effect of Na/Ca adsorbents on NiRu-DFM performance for integrated CO_2 capture and hydrogenation, *Energy Fuels*, 2024, **38**, 21204–21218.

32 A. I. Tsiotsias, N. D. Charisiou, A. G. S. Hussien, A. A. Dabbawala, V. Sebastian, K. Polychronopoulou and M. A. Goula, CO_2 capture and methanation using $Ru/Na_2O/Al_2O_3$ dual-function materials: Effect of support synthesis method and Ru load, *J. Environ. Chem. Eng.*, 2024, **12**, 112712.

33 A. I. Tsiotsias, E. Harkou, N. D. Charisiou, V. Sebastian, D. R. Naikwadi, B. van der Linden, A. Bansode, D. Stoian, G. Manos, A. Constantinou and M. A. Goula, Very low Ru loadings boosting performance of Ni-based dual-function materials during the integrated CO_2 capture and methanation process, *J. Energy Chem.*, 2025, **102**, 309–328.

34 C. Vandelois, *Optimization of DFMS (Dual Function Materials) for Combined CO_2 Capture and Methanation*, Université catholique de Louvain, Faculté des bioingénieurs, 2023.

35 A. I. Tsiotsias, N. D. Charisiou, A. G. S. Hussien, V. Sebastian, K. Polychronopoulou and M. A. Goula, Integrating capture and methanation of CO_2 using physical mixtures of $Na\text{-}Al_2O_3$ and mono-/bimetallic (Ru)Ni/Pr-CeO_2, *J. Chem. Eng.*, 2024, **491**, 151962.

36 M. S. Duyar, S. Wang, M. A. Arellano-Treviño and R. J. Farrauto, CO_2 utilization with a novel dual function material (DFM) for capture and catalytic conversion to synthetic natural gas: An update, *J. CO2 Util.*, 2016, **15**, 65–71.

37 L. R. Karadaghi, E. M. Williamson, A. T. To, A. P. Forsberg, K. D. Crans, C. L. Perkins, S. C. Hayden, N. J. LiBretto, F. G. Baddour, D. A. Ruddy, N. Malmstadt, S. E. Habas and R. L. Brutchey, Multivariate Bayesian optimization of CoO nanoparticles for CO_2 hydrogenation catalysis, *J. Am. Chem. Soc.*, 2024, **146**, 14246–14259.

38 S. Lim, H. Lee, H. S. Kim, J. S. Shin, J. M. Lee and D. H. Kim, Bayesian-optimization-based design of highly active and stable Fe-Cu/SSZ-13 catalysts for the selective catalytic reduction of NO_x with NH_3, *React. Chem. Eng.*, 2024, **9**, 3029–3037.

39 A. Ramirez, E. Lam, D. Pacheco, Y. Hou, H. Tribukait, L. Roch, C. Copéret and P. Laveille, Accelerated exploration of heterogeneous CO_2 hydrogenation catalysts by Bayesian optimized high-throughput and automated experimentation, *Chem Catal.*, 2023, **4**, 100888.

40 C. Wei, H. Ding, Z. Zhang, F. Lin, Y. Xu and W. Pan, Research progress of bimetallic catalysts for CO_2 hydrogenation to methane, *Int. J. Hydrogen Energy*, 2024, **58**, 872–891.

41 C. Jeong-Potter, A. Zangiabadi and R. Farrauto, Extended aging of Ru-Ni, Na_2O/Al_2O_3 dual function materials (DFM) for combined capture and subsequent catalytic methanation of CO_2 from power plant flue gas, *Fuel*, 2022, **328**, 125283.

42 J. He, S. Chang, H. Du, B. Jiang, W. Yu, Z. Wang, W. Chu, L. Han, J. Zhu and H. Li, Efficient hydrogenation of CO_2 to formic acid over amorphous NiRuB catalysts, *J. CO2 Util.*, 2021, **54**, 101751.

43 A. Bermejo-López, B. Pereda-Ayo, J. A. Onrubia-Calvo, J. A. González-Marcos and J. R. González-Velasco, Boosting dual function material $Ni\text{-}Na/Al_2O_3$ in the CO_2 adsorption and hydrogenation to CH_4: Joint presence of Na/Ca and Ru incorporation, *J. Environ. Chem. Eng.*, 2023, **11**, 109401.

44 C. Crisafulli, S. Scirè, S. Minicò and L. Solarino, Ni-Ru bimetallic catalysts for the CO_2 reforming of methane, *Appl. Catal., A*, 2002, **225**, 1–9.

45 O. U. Valdés-Martínez, V. A. Suárez-Toriello, J. A. de los Reyes, B. Pawelec and J. L. G. Fierro, Support effect and metals interactions for $NiRu/Al_2O_3$, TiO_2 and ZrO_2 catalysts in the hydrodeoxygenation of phenol, *Catal. Today*, 2017, **296**, 219–227.

46 M. A. Arellano-Treviño, N. Kanani, C. W. Jeong-Potter and R. J. Farrauto, Bimetallic catalysts for CO_2 capture and hydrogenation at simulated flue gas conditions, *J. Chem. Eng.*, 2019, **375**, 121953.

47 J. Zeng, Y. Yao, F. Wang, J. Gao, L. Zhang, G. Xu, Z. Zhong and F. Su, Enhanced CO_2 methanation through electronic modification of Ru to Ni in Ni-Al hydrotalcite-derived catalysts, *Green Energy Environ.*, 2024, **12**, 006.

48 M. I. Qadir, F. Bernardi, J. D. Scholten, D. L. Baptista and J. Dupont, Synergistic CO_2 hydrogenation over bimetallic Ru/Ni nanoparticles in ionic liquids, *Appl. Catal., B*, 2019, **252**, 10–17.

49 L. P. Merkouri, E. le Saché, L. Pastor-Pérez, M. S. Duyar and T. Ramirez Reina, Versatile Ni-Ru catalysts for gas phase CO_2 conversion: Bringing closer dry reforming, reverse water gas shift and methanation to enable end-products flexibility, *Fuel*, 2021, **315**, 123097.

50 L. Proaño, M. A. Arellano-Treviño, R. J. Farrauto, M. Figueredo, C. Jeong-Potter and M. Cobo, Mechanistic assessment of dual function materials, composed of Ru-Ni, Na_2O/Al_2O_3 and Pt-Ni, Na_2O/Al_2O_3, for CO_2 capture and methanation by in-situ DRIFTS, *Appl. Surf. Sci.*, 2020, **533**, 147469.

51 R. Kumar, H. Miyaoka, K. Shinzato and T. Ichikawa, Analysis of sodium generation by sodium oxide decomposition on corrosion resistance materials: A new approach towards sodium redox water-splitting cycle, *RSC Adv.*, 2021, **11**, 21017–21022.

52 Q. Liu, S. Wang, G. Zhao, H. Yang, M. Yuan, X. An, H. Zhou, Y. Qiao and Y. Tian, CO_2 methanation over ordered mesoporous NiRu-doped $CaO\text{-}Al_2O_3$ nanocomposites with enhanced catalytic performance, *Int. J. Hydrogen Energy*, 2018, **43**, 239–250.

53 N. Yao, H. Ma, Y. Shao, C. Yuan, D. Lv and X. Li, Effect of cation-oligomer interactions on the size and reducibility of NiO particles on $NiRu/SiO_2$ catalysts, *J. Mater. Chem.*, 2011, **21**, 17403–17412.

54 L. P. Merkouri, A. I. Paksoy, T. R. Reina and M. S. Duyar, The need for flexible chemical synthesis and how dual-function materials can pave the way, *ACS Catal.*, 2023, **13**, 7230–7242.

55 A. Bermejo-López, B. Pereda-Ayo, J. A. González-Marcos and J. R. González-Velasco, Modeling the CO_2 capture and in situ conversion to CH_4 on dual function $Ru\text{-}Na_2CO_3/Al_2O_3$ catalyst, *J. CO2 Util.*, 2020, **42**, 101351.

56 A. Bermejo-López, B. Pereda-Ayo, J. A. González-Marcos and J. R. González-Velasco, Ni loading effects on dual function materials for capture and in-situ conversion of CO_2 to CH_4 using CaO or Na_2CO_3, *J. CO2 Util.*, 2019, **34**, 576–587.
57 S. Cimino, E. M. Cepollaro, L. Lisi, S. Fasolin, M. Musiani and L. Vázquez-Gómez, Ru/Ce/Ni metal foams as structured catalysts for the methanation of CO_2, *Catalysts*, 2021, **11**, 1–15.
58 S. A. Sreenavya, B. T. Baskaran, G. V. Ganesh, S. D. Sharma, N. Kulal and S. A. Sakthivel, Framework of ruthenium-containing nickel hydrotalcite-type material: Preparation, characterisation, and its catalytic application, *RSC Adv.*, 2018, **8**, 25248–25257.
59 L. P. Merkouri, J. L. Martín-Espejo, L. F. Bobadilla, J. A. Odriozola, M. S. Duyar and T. R. Reina, Flexible NiRu systems for CO_2 methanation: From efficient catalysts to advanced dual-function materials, *Nanomaterials*, 2023, **13**, 506.
60 M. Danielis, L. P. Merkouri, A. Braga, A. Trovarelli, M. S. Duyar and S. Colussi, Feasibility of green mechanochemical synthesis for dual function materials preparation, *J. CO2 Util.*, 2024, **86**, 102895.
61 H. C. Wu, T. C. Chen, J. H. Wu, C. W. Pao and C. S. Chen, Influence of sodium-modified Ni/SiO_2 catalysts on the tunable selectivity of CO_2 hydrogenation: Effect of the CH_4 selectivity, reaction pathway and mechanism on the catalytic reaction, *J. Colloid Interface Sci.*, 2021, **586**, 514–527.
62 Z. Zhang, Y. Guo, J. Chu, P. Huang, P. Kong, J. Sun, R. Wang, W. Li and C. Zhao, Integrated CO_2 capture and conversion performance of Ni-CaO dual functional materials pellets in O_2-containing flue gas stream, *Chem. Eng. Sci.*, 2025, **306**, 121241.
63 A. Bermejo-López, B. Pereda-Ayo, J. A. Onrubia-Calvo, J. A. González-Marcos and J. R. González-Velasco, Aging studies on dual function materials Ru/Ni-Na/Ca-Al_2O_3 for CO_2 adsorption and hydrogenation to CH_4, *J. Environ. Chem. Eng.*, 2022, **10**, 107951.
64 M. Peng, R. Han, L. Wei, Y. Wang, Z. Li, H. Yan, G. Han and Q. Liu, Cu promoted Ni-Ca dual functional materials for integrated CO_2 capture and utilization in O_2-containing flue gas: Eliminating the delay in the utilization stage, *Sep. Purif. Technol.*, 2024, **354**, 129516.
65 M. J. Lashaki, S. Khiavi and A. Sayari, Stability of amine-functionalized CO_2 adsorbents: A multifaceted puzzle, *Chem. Soc. Rev.*, 2019, **48**, 3320–3405.
66 K. Kawai, T. Fukuda, Y. Nakano and K. Takeshita, Thermal decomposition analysis of simulated high-level liquid waste in cold-cap, *EPJ Nucl. Sci. Technol.*, 2016, **2**, 44.
67 The GPyOpt A Bayesian optimization framework in python, **https://github.com/SheffieldML/GPyOpt**, accessed date, November 2024.